Journal of Materials Chemistry A

PAPER

Novel Li_3ClO based glasses with superionic properties for lithium batteries

Cite this: DOI: 10.1039/c3ta15087a

M. H. Braga,[a] J. A. Ferreira,[b] V. Stockhausen,[c] J. E. Oliveira[d] and A. El-Azab[e]

Received 8th December 2013
Accepted 26th January 2014

DOI: 10.1039/c3ta15087a

www.rsc.org/MaterialsA

Three types of next generation batteries are currently being envisaged among the international community: metal-air batteries, multivalent cation batteries and all-solid-state batteries. These battery designs require high-performance, safe and cost effective electrolytes that are compatible with optimized electrode materials. Solid electrolytes have not yet been extensively employed in commercial batteries as they suffer from poor ionic conduction at acceptable temperatures and insufficient stability with respect to lithium-metal. Here we show a novel type of glasses, which evolve from an antiperovskite structure and that show the highest ionic conductivity ever reported for the Li-ion (25 mS cm^{-1} at 25 °C). These glassy electrolytes for lithium batteries are inexpensive, light, recyclable, non-flammable and non-toxic. Moreover, they present a wide electrochemical window (higher than 8 V) and thermal stability within the application range of temperatures.

Introduction

In lithium-ion batteries the safety issue remains a major barrier. Battery manufacturers are now able to produce high-quality lithium-ion cells for consumer electronics, with less than one reported safety incident for every one million cells produced.[2] However, this failure rate is still too high for applications in plug-in hybrid electric vehicles and pure electric vehicles, since several hundreds of lithium-ion cells will be needed to power a vehicle. The failure of a single cell can generate a large amount of heat and flame, both of which can then trigger thermal runaway of neighbouring cells, leading to failure throughout the battery pack. Consequently, there is a wide effort to tackle the safety issue of lithium batteries.[2] Chen and co-workers[3] showed that a higher graphite negative electrode surface area in a lithium-ion cell can result in a more solid electrolyte interphase (SEI) and therefore more heat generation during thermal decomposition. This initial reaction, which occurs at ~110 °C, can further trigger other exothermal reactions in the cell. Therefore, the latest work on graphitic anodes mainly focuses on the development of a stable artificial solid electrolyte interphase to stabilize the lithiated graphite and improve both safety and cycling performance.

Recently, lithium batteries using oxygen from air at the positive electrode (lithium-air batteries) have attracted worldwide attention. In this open system, the use of electrolytes with low volatility is strictly required. For lithium-air batteries a major focus of attention has been the lithium-metal anode protected by a lithium-ion conducting ceramic electrolyte.[2] LISICON ($Li_{(1+x+y)}Al_xTi_{2-x}Si_yP_{(3-y)}O_{12}$)[4] has been used for the previous purpose with a major inconvenient related to – LISICON being reduced in contact with Li-metal – following-on a Li/ceramic interface difficult to cycle.[2]

Promising results were recently obtained with a $Li_{10}GeP_2S_{12}$ solid electrolyte.[5] In this solid electrolyte medium, Li^+ ions are conducted at 0.012 mS cm^{-1} and 12 mS cm^{-1} at −100 °C and 25 °C, respectively, which is considered to be a high conductivity. Mo *et al.*[6] found that $Li_{10}GeP_2S_{12}$ is not stable against reduction by lithium at low voltage or extraction of Li with decomposition at high voltage.

On a different front, sulfide glasses have been studied due to their high ionic conductivity. A glass of the Li_3PO_4–Li_2S–SiS_2 system is formed at ambient pressure by quenching $0.03Li_3PO_4$–$0.59Li_2S$–$0.38SiS_2$ in liquid nitrogen. Its conductivity at room temperature is 0.69 mS cm^{-1} (ref. 7) and its stability against electrochemical reduction is as wide as 10 V.[8]

We have developed and optimized a glassy electrolyte with ultra-fast ionic conduction based on an antiperovskite $Li_{3-2x}M_xHalO$ structure, in which M is a higher valent cation such as Mg^{2+}, Ca^{2+} or Ba^{2+} and Hal is a halide like Cl^- or I^- or a mixture of halides.

The glass–liquid transition is the reversible transition in amorphous materials from a hard and relatively brittle state into a molten or rubber-like state.[9] The glass transition of a liquid to a solid-like state may occur with either cooling or

[a]CEMUC and Engineering Physics Department, Engineering Faculty, Porto University, Portugal
[b]Energy and Geology National Laboratory, S. Mamede Infesta, Portugal
[c]Engineering Physics Department, Engineering Faculty, Porto University, Portugal
[d]CFP and Engineering Physics Department, Engineering Faculty, Porto University, Portugal
[e]School of Nuclear Engineering and School of Materials Engineering, Purdue University, USA

compression.[10] The transition comprises a relatively smooth increase in the viscosity of the material of about 17 orders of magnitude[11] without any pronounced change in the material structure. The consequence of this dramatic increase is a glass exhibiting solid-like mechanical properties on the timescale of practical observation. While glasses are often thought of as rigid and completely immobile, it is well known that relaxation processes of one type or another continue to be measurable all the way down to the cryogenic range. Hundreds of degrees below T_g, on the other hand, there is frequently an important source of dielectric loss in ordinary glass insulators. This is attributed to mobile alkali ions and, to a lesser extent, protons, in the anionic network. In many cases, for example in solid electrolytes, these quasi-free modes of motion are the focus of special materials interest such as advanced solid electrolytes based on freely mobile cations.[11]

A more operative classification for the glass transition temperature is that at this temperature – or within a few degrees – the specific heat, the coefficient of thermal expansion and eventually the dielectric constant change abruptly. In the Differential Scanning Calorimetry (DSC) experiment, T_g is expressed by a change in the base line, indicating a change in the heat capacity of the material. No enthalpy (latent heat change) is associated with this transition (it is a second order transition); therefore, the effect in a DSC curve is slender and is distinguishable only if the instrument is sensitive. These solid electrolytes undergo a viscous liquid to a solid-like transition, at T_g. Above T_g a non-Arrhenius conductivity regime is observed [$T_g(Li_3ClO) \approx 119$ °C, $T_g(Li_{3-2\times0.005}Mg_{0.005}ClO) \approx 109$ °C, $T_g(Li_{3-2\times0.005}Ca_{0.005}ClO) \approx 99$ °C, $T_g(Li_{3-2\times0.005}Ba_{0.005}ClO) \approx 75$ °C, $T_g(Li_{3-2\times0.005}Ba_{0.005}Cl_{0.5}I_{0.5}O) \approx 38$ °C]. One variant of the solid electrolyte developed by us, $Li_{3-2x}Ba_xClO$ ($x = 0.005$), has a conductivity of 25 mS cm^{-1}, 38 mS cm^{-1} and 240 mS cm^{-1} at 25 °C, 75 °C and 100 °C, respectively, in the glassy state or the supercooled liquid state. Another variant, $Li_{3-2x}Ba_xCl_{0.5}I_{0.5}O$ ($x = 0.005$), has a conductivity of 121 mS cm^{-1} at 50 °C in the supercooled liquid state. Typically, the conductivity of liquid electrolytes at room temperature (20 °C) is about 10 mS cm^{-1}, and it increases by approximately 30–40% at 40 °C. The calculated electronic energy band gap is 6.44 eV for the base crystalline material, Li_3ClO, which does not change more than the decimal value of an eV with low dopant levels up to 0.7 at%. Cyclic voltammetry experiments with glassy samples at 130 °C have shown a stability range of more than 8 V, which allows the application of our electrolyte in next generation high voltage battery cells (5 V).

Antiperovskite hydroxides, most of them following the general formula $Li_{3-n}(OH_n)Hal$[12–14] or $Li_4(OH)_3Cl$[15] present ionic conductivities which are considerably smaller than the $Li_{3-2\times x}M_xHalO$ vitreous electrolytes, achieving the highest ionic conductivity, 0.010 S cm^{-1}, at ~250 °C (for $Li_5(OH)_3Cl_2$). Nevertheless, they were observed in our samples prior to the formation of the glasses and they may have an important role in glass formation since the translational symmetry characteristic of a homogeneous fluid is broken by exposure to an external force field, in the vicinity of a confining surface (which may be regarded as the source of an external field), or in the presence of an interface between coexisting phases.[10]

Experimental

Synthesis, characterization and neutron scattering

The preparation of Li_3ClO and corresponding doped solid electrolyte samples consisted in pre-drying LiCl, and Li, Mg, Ca or Ba hydroxides since most of them are highly hygroscopic, weighing the stoichiometric amounts and mixing them. Then, by adding a few drops of deionized water, a paste was formed and introduced in a Teflon reactor, which was firmly closed. The reactor was heated at 220–240 °C for at least 4 days before it was opened to let the water evaporate for approximately 1 h. Then it was closed in glassware and allowed to cool to room temperature. A vacuum pump was used to dry the water out. A few hours are needed for the sample to become 100% Li_3ClO crystalline or its doped homolog. We have obtained powders and if they were too dry we could not obtain the glassy sample even after 5–6 heating/cooling Electrochemical Impedance Spectroscopy (EIS) cycles. Pellets were obtained as well (with a cold press). These pellets did not work out, not only because the powders were too dry, but also because we could not press the pellets enough during heating/cooling cycles since they would break.

The part of the sample designated for EIS experiments was manipulated in air, after synthesis, since it proportionated the formation of hydroxides that were beneficial to glass formation.

The cooling process took place in the sand bath, it was slow, in the screw pressed cell, and most of the times EIS experiments were performed during cooling. Glasses were obtained after hydroxides ran out (eventually this phase works as a confining surface, helping glass formation).

Samples were submitted to X-ray Diffraction (XRD) in a PANalytical instrument, using CuK$_\alpha$ radiation, to determine the amount of the product present in the sample as observed in Fig. 1. XRD measurements were also performed after EIS experiments to determine if the material was amorphous. An

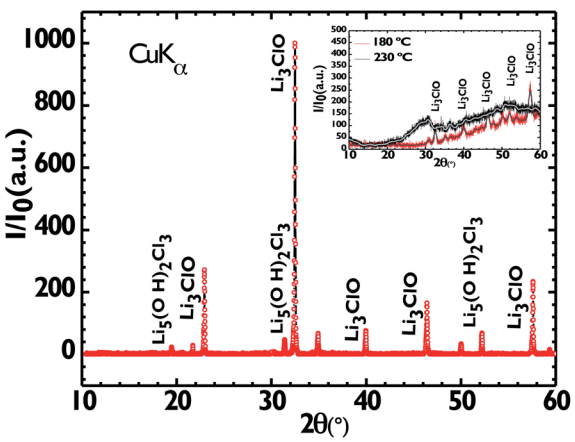

Fig. 1 XRD diffractogram of a sample of Li_3ClO at room temperature. There is evidence of a small amount of a hydroxide phase, possibly $Li_5(OH)_2Cl_3$,[14] due to sample manipulation. At 180 °C (graph right above), there is little evidence of the hydroxide but the presence of crystalline Li_3ClO is still clear, although an amorphous phase becomes visible. At 230 °C (graph right above), only an amorphous phase is clearly distinguishable. The XRD radiation used was CuK$_\alpha$.

example of the latter measurements can be observed in Fig. 2. The crystal structures and lattice parameters of the solid electrolytes were calculated for the first time, at the ground state and elevated temperatures using first principles. Simulations of the XRD patterns were also obtained to compare with the experimental ones. Mg, Ca or Ba quantitative analysis was performed by means of Atomic Absorption Spectroscopy (AAS).

The high sensitivity of ionic conductivity of glasses to chemical composition is well known, therefore different doping elements and compositions $Li_{3-2\times x}M_xHalO$ ($x = 0$ in Li_3ClO; $x = 0.002$, 0.005, 0.007 and 0.01 for M = Mg and Ca; $x = 0.005$ for M = Ba and Hal = Cl or Hal = 0.5Cl + 0.5I) were synthesized. To obtain glasses, we mounted our samples into our gold cell (described in ionic and electronic conductivity measurements), in an air atmosphere, and performed heating–cooling cycles up to 250 °C. Eventually, after the first heating–cooling cycle (the sample was slowly cooled down and protected from moisture), the ionic conductivity grows abruptly.

Differential Scanning Calorimetry experiments (DSC) in alumina closed crucibles and an Ar flowing atmosphere, using dried powder and slightly pressed powder, show that after the first cycle, the hydroxide's melting peak cannot be distinguished anymore. The latter also shows a baseline anomaly that is probably due to the glassy transition and a clear first order transition corresponding to the melting peak of $Li_{3-0.01}Mg_{0.005}ClO$ as it can be distinguished in Fig. 3. A Labsys-Setaram instrument was used to perform the latter measurements.

The role of the lattice during hopping and diffusion was established by means of neutron inelastic incoherent scattering (IINS). A sample holder stick and a lithium-metal symmetric battery cell (screw brass collectors, a quartz glass tube with approximately 2.5 cm of diameter, and about 3 cm of sample – distance between lithium electrodes) were prepared for these experiments at the Los Alamos Neutron Scattering Center (LANSCE). Temperature, current and applied frequency could vary.

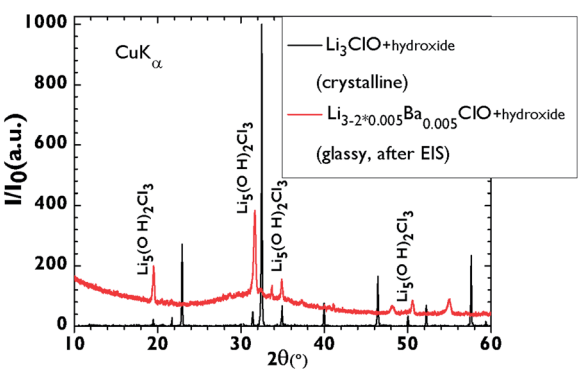

Fig. 2 XRD diffractogram of a Li_3ClO – crystalline sample (the same as in Fig. 1) and of a $Li_{3-2\times0.005}Ba_{0.005}ClO$ – glassy sample at room temperature after EIS measurements (after six cycles of heating/cooling). Compton's scatter, which is inelastic scattering and amorphous scatter related to the glass is observed. There is evidence of the presence of a hydroxide phase, possibly $Li_5Cl_3(OH)_2$ (ref. 14) (the same as in Fig. 1), that due to sample's air exposed manipulation is inevitable and starts to form at the surface.

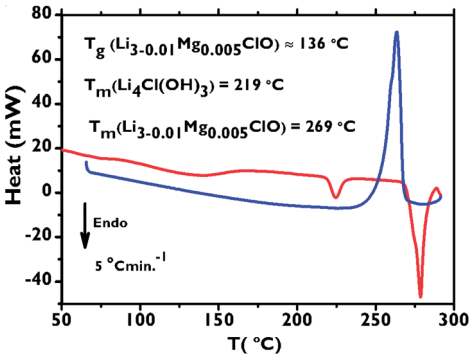

Fig. 3 Differential Scanning Calorimetry (DSC). DSC curves for a sample of $Li_{3-2\times0.005}Mg_{0.005}ClO$ during heating and cooling, at 5 °C min^{-1}, eventually showing the glass transition (baseline anomaly) and first order transition temperatures (melting corresponds to endothermic incidents (heating curve) and to an exothermic incident on the cooling curve).

Ionic and electronic conductivity measurements

Electrochemical Impedance Spectroscopy (EIS) was performed in a cell using either gold or stainless steel (blocking electrodes) that was heated up in a sand bath, in an air atmosphere or in a glovebox in Ar and/or air (water vapour < 10%). Our gold symmetric cell has about 1.77 cm^2 of surface area. It consists of two disk foils of gold separated by the sample with a thickness of about less than 5 mm (usually 1–3.0 mm) and it was pressed tightly with a screw. Our stainless steel cell was bulky and could contain a sample with the same dimensions as the gold one. In the latter cell, blocking electrodes could be stainless steel or copper (just for temperatures near room temperature). This cell was seldom used. The instrument used is a Bio-Logic SP240. Experiments were conducted in the temperature range of 25 to 255 °C. The frequency range was 5 MHz–0.1 Hz. Ionic conductivity was calculated using Nyquist impedance of an equivalent circuit containing a passive resistance in series with a constant phase element in series with a circuit containing a capacitor in parallel with a resistance. The latter resistance is the solid electrolyte's resistance which plays the role of the dielectric in an ideal parallel-plate capacitor. When the resistance to ionic conduction becomes too small and Faraday's induction caused by the cables is unavoidable and prominent at high frequencies, a non-ideal inductive element was added in series to the previous circuit. Fig. 4 and 5 show EIS measurement data for a sample containing $Li_{3-0.005}Ba_{0.005}ClO$ tested in a symmetric gold cell as previously described, for different cycles and temperatures. Tests in the empty cell and with AgI were performed to control the procedures and establish analysis methods.

Cyclic voltammetry tests were performed in the stainless steel cell with a lithium electrode as a reference electrode and a counter electrode of copper or stainless steel. Chronopotentiometry was performed in a lithium symmetric cell equivalent to the gold one previously described. Three measurements intercalated by an open circuit interval were performed containing 20 cycles each of 40 min. (20 min at a positive current and 20 min at a negative current). Measurements were performed in an Ar-dry glovebox.

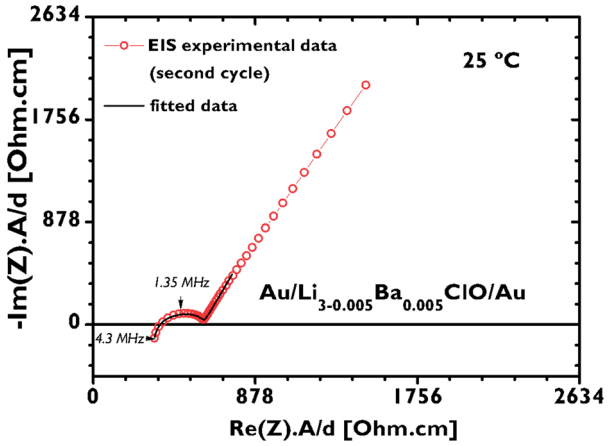

Fig. 4 EIS experimental and fitted data using the equivalent circuit previously described. Nyquist impedance and corresponding fitting curve for the 2nd cycle of a sample containing $Li_{3-0.005}Ba_{0.005}ClO$, at 25 °C. *A* is the surface area, $A = 1.76\ cm^2$ and *d* the thickness, $d = 0.2$ cm.

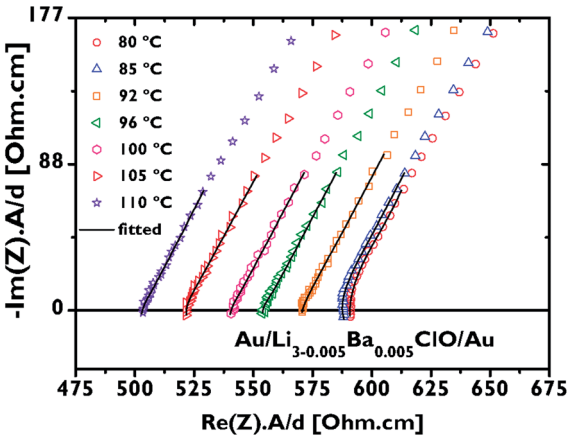

Fig. 5 EIS experimental and fitted data using the equivalent circuit previously described. Nyquist impedance for the 2nd cycle of a sample containing $Li_{3-0.005}Ba_{0.005}ClO$, at different temperatures after the glass transition. *A* is the surface area and *d* the thickness.

Calculations

Density Functional Theory (DFT) calculations with Projector Augmented Wave (PAW) pseudopotentials[16] as implemented in the Vienna *Ab initio* Simulation Package (VASP) code,[17] were performed. A plane wave cutoff of 500 eV, and a k-mesh of 4 × 4 × 4 were used. Calculations were implemented in real space and were performed within the *P*1 space group supercells containing at least 134 atoms. Some supercells contained as many atoms as possible, 270 atoms or more, to allow better approximations with the real Ba^{2+}, Ca^{2+} or Mg^{2+} concentrations. The Generalized Gradient Approximation (GGA), and the Perdew–Burke–Ernzerhof (PBE) functional[18] were used, and no magnetic moments were included in the model. The Heyd–Scuseria–Erznerhof (HSE06) functional[19] was used to calculate the band structure and electronic Density of States (DOS) to determine the lowest unoccupied molecular orbital (LUMO) and the highest occupied molecular orbital (HOMO).

The Phonon direct method[20] was used to predict the lattice dynamics using the quasi-harmonic approximation on the VASP minimized structures that had the lowest ground state energy.

The Nudged Elastic Band Method (NEB)[21] was used to calculate the transition state energy as a function of the reaction coordinate for different configurations.

Results and discussion

Ionic conduction in solids occurs by ion hopping from a crystal lattice site to another by the vacancy mechanism; therefore it is necessary to have a partial occupancy of energetically equivalent or near-equivalent sites. In favourable structures, the defects may be mobile, leading to high ionic conductivity. While the rate of ion transport in a crystalline solid is dictated by the diffusivity and concentration of the vacancies mediating ion transport, the open structure of inorganic glassy materials facilitates the process of ionic hopping and results in enhanced conductivity. Inorganic glasses thus represent an attractive material class for electrolyte applications. An advantage of inorganic glasses is single-cation conduction; they belong to the so-called decoupled systems in which the mode of ionic conduction relaxation is decoupled from the mode of structural relaxation.[22]

Comparing the temperature dependence of the relaxation time of the structure and conduction for inorganic glassy liquids with, say, organic polymers shows that the former exhibit a decoupling character capable of yielding higher single ion conduction in the glassy state. Single cation conduction is associated with fewer side reactions and significantly wider electrochemical stability windows[11] which can be up to 10 V.[8]

Fig. 6a and b show the antiperovskite crystal structure and lattice parameter of Li_3ClO, which was the material base for the synthesis of the glass shown in Fig. 7.

The structural, lattice dynamics and thermodynamic properties of the solid antiperovskite are described here for the first time. We have used Density Functional Theory (DFT) and

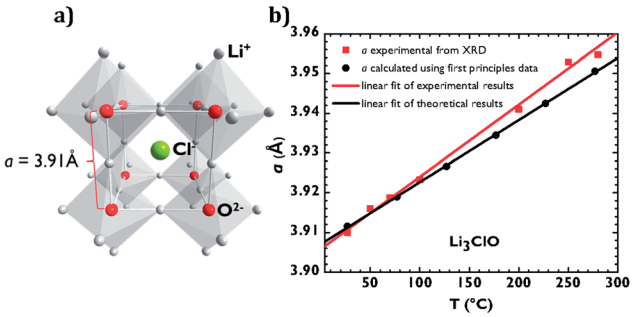

Fig. 6 The crystal structure of a Li_3ClO antiperovskite cubic $Pm\bar{3}m$. (a) The cube has a halogen ion at the center, and six octahedra centered about the vertex ions of O^{2-}. Li^+ occupies the vertex sites of the octahedra. When a higher valent cation, *e.g.* Ca^{2+}, substitutes one Li^+ cation, a vacancy is formed. (b) Li_3ClO lattice parameter as a function of temperature (experimental and calculated).

Fig. 7 Photograph of a glassy sample of $Li_{3-2\times0.005}Ca_{0.005}ClO$.

phonon analysis. Nevertheless, the crystal structure and the ionic conductivity of Li_3ClO and $Li_3Cl_{0.5}Br_{0.5}O$ – in their crystalline states – were described recently by Zhao and Daemen[23] and Zhang *et al.*[24] who performed DFT calculations and molecular dynamics simulations to characterize Li-ion diffusion in the antiperovskite crystal structure of Li_3ClO and $Li_3Cl_{0.5}Br_{0.5}O$. The lattice parameter for the primitive cubic $Pm\bar{3}m$ crystal structure of Li_3ClO (*space group number*: 221, *Pearson symbol*: cP5), a, was found in this work to be 3.91 Å at room temperature as observed in Fig. 6, which is in very good agreement with the experimental results in ref. 23 and the calculations in ref. 24 and the thermal expansion coefficient was found to be $\alpha = 4.65 \times 10^{-5}\ ^{\circ}C^{-1}$ which is higher than $\alpha = 2.11 \times 10^{-5}\ ^{\circ}C^{-1}$ in[24] but in very good agreement with our experimental results in Fig. 6b. Eventually a part of Li_3ClO was amorphous, at $T > 120$ °C, justifying the small deviation from the experimental to the calculated lattice parameters in Fig. 6b.

DFT was also used to understand the role of higher valent cation doping in both the crystalline and amorphous states. In Fig. 8, four snapshots of the Ca^{2+} doped structure and Coulomb equilibria during Li^+ hopping highlight the lattice dynamics leading to further disorder during diffusion that might have an additional role in the crystal–amorphous transition. This disorder was also described by Zhang *et al.*[24] who found the phases Li_3ClO and $Li_3Cl_{0.5}Br_{0.5}O$ to be metastable. In fact, they predicted a transition that will drastically make the volume rise at ~150 °C. We think that this transition is the glass transition of these compounds which is in agreement with the results presented here for Li_3ClO. Moreover, they present a calculated Li-ion conductivity of 0.12 mS cm^{-1} for Li_3ClO at 27 °C (300 K), which is not in agreement with Zhao and Daemen[23] (who obtained 0.85 mS cm^{-1}), but totally in agreement with the value we have obtained for Li_3ClO – solid-like by extrapolation of our experimental data for 27 °C.

In Li_3ClO antiperovskite, the center of the cube is occupied by Cl^- and the center of the octahedra is occupied by O^{2-}. Li^+ ions occupy the vertices of the octahedra; leading to a Li-rich structure as shown in Fig. 6a. Doping with higher valent cations, like Ca^{2+}, creates vacancies in the cation sublattice, one per Ca^{2+} ion, to satisfy charge balance. The vacancy creation by means of doping lowers the activation energy for Li-ion diffusion and, as a result, leads to faster ion transport. The latter effect is shown in Fig. 9a.

At lower temperatures where conduction's extrinsic regime applies, vacancies will fall near doping cations thus forming impurity–vacancy complexes as the one shown in Fig. 9a. Fig. 9b shows activation energies for the latter type of complexes, which were calculated and obtained experimentally, and do not surpass 0.6 eV.

At higher temperatures, in the intrinsic regime, however, vacancies will separate from the doping ion and the activation barriers for ion hopping will reach 1.58 eV. As the solid-like state becomes a liquid state at higher temperatures, the latter effect was not experimentally observed.

In the Arrhenius regime, the ionic conductivity, obtained experimentally, shows activation energies of 0.42 and 0.46 eV for $Li_{3-2\times0.005}Ca_{0.005}ClO$ and $Li_{3-2\times0.005}Mg_{0.005}ClO$, respectively. We notice here that the presence of M^{2+} (Mg, Ca and Ba) ions induces anisotropy in the lattice, causing ion currents to flow more in the direction of the lower activation energy, as illustrated in Fig. 9 and as expected.

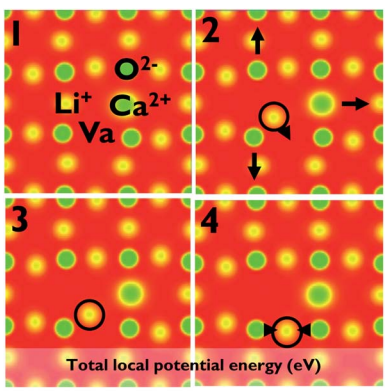

Fig. 8 Li^+ diffusion and correspondent lattice dynamics. From 1 to 4 it can be seen how the lattice adjusts during diffusion.

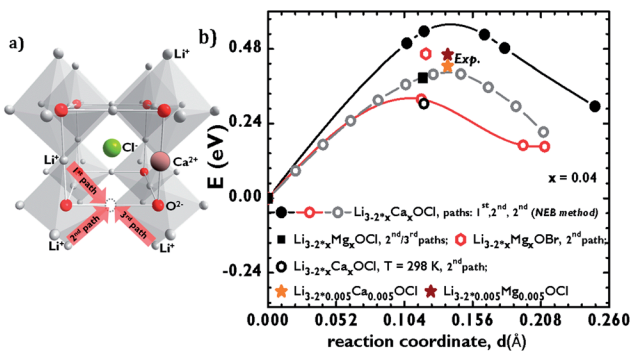

Fig. 9 (a) Crystal structure of Li_3ClO antiperovskite highlighting the formation of a vacancy and three different paths for Li^+ diffusion, after being doped with Ca^{2+}. (b) Activation energies for different paths in (a), dopants and temperatures calculated by DFT-GGA and the Nudged Elastic Band (NEB)[21] method as implemented in VASP code[17] and Phonon,[20] compared with the experimental values obtained in the solid-like (Arrhenius) regime for $Li_{3-2\times0.005}M_{0.005}ClO$ (M = Ca, Mg, Ba).

For Li_3ClO, we have obtained an activation energy of 0.49 eV which is in agreement with the calculated results in ref. 24 and higher than 0.26 eV which was obtained experimentally in ref. 23.

Electronic properties, such as the band structure and Density of States (DOS) were also calculated by means of DFT using the GGA functionals[16,18] and the Hyed–Scuseria–Erznerhof (HSE06) functionals.[19] In Fig. 10a, electronic band structure calculations using GGA as well as the correspondent band gap of 4.74 eV are shown. Fig. 10b shows a HSE06 calculation and its correspondent band gap, E_g, value of 6.44 eV, which indicates a wide range of electrochemical stability for the crystalline material. Zhang *et al.*[24] have also calculated DOS using similar methods and found a band gap of 5 eV which is in agreement with our DFT-GGA calculation. Referring to the method section, the band gap calculated using the HSE06 hybrid functional seems to agree more with experiments than the one calculated using the GGA functional as generally expected.[6] Fig. 10c shows voltammetry graphs correspondent to four experiments in which it can be observed that no substantial oxidation of Li_3ClO or $Li_{3-2\times0.005}Ba_{0.005}ClO$ at 130 °C can be detected up to 8 V, which covers all the negative–positive electrode-pair voltage windows for Li batteries. The electrical conductivity was obtained from these voltammetry cycles using the Hebb–Wagner (H–W) method.[25] In a polarization measurement, under steady state conditions, in a $Li/Li_3ClO/Cu$ cell with an ion blocking electrode such as Cu, $\partial I/\partial V = -A\sigma_e/d$ where I is the electrical current, V is the applied voltage (E in Fig. 10c), A the cross-sectional area of the electrolyte (with $j = I/A$), d the thickness of the electrolyte and σ_e its electronic conductivity. The derivative $\partial I/\partial V$ yields the electronic conductivity in the electrolyte near the end adjacent to the blocking electrode.

For Li_3ClO at 130 °C in the 1.4–2.5 V interval, $\sigma_e = 9.2 \times 10^{-9}$ S cm^{-1}, and in the interval 2.55–2.82 V, $\sigma_e = 1.18 \times 10^{-7}$ S cm^{-1}. For $Li_{3-2\times0.005}Ba_{0.005}ClO$ at 130 °C for the first cycle and over the interval 4.1–5.97 V, $\sigma_e = 6.77 \times 10^{-8}$ S cm^{-1}. For the second cycle, and in the range 2.07–5.37 V, $\sigma_e = 1.05 \times 10^{-8}$ S cm^{-1}. The latter yields a transport number, $t_i = \sigma_i/(\sigma_i + \sigma_e)$, near unity as required for good quality solid electrolytes; σ_i is the ionic conductivity.

From our experimental study and DFT analysis, we observed that the ionic radius of the doping atom plays an important role in the liquid/solid-like transition; namely, the larger the doping ion radius the lower the glass transition temperature as it is shown in Fig. 11. This effect arises due to the disorder that the impurity introduces in the crystal structure as appreciated in Fig. 8, especially the part related to the enthalpy. Consequently,

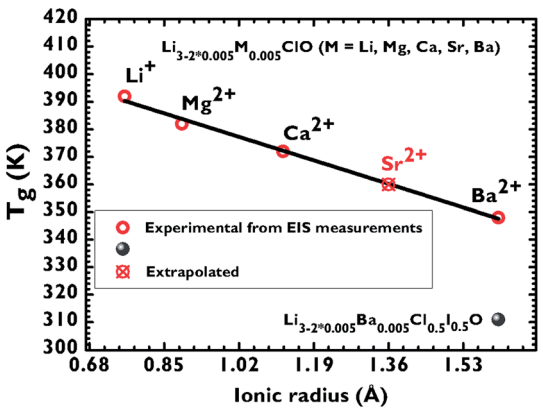

Fig. 11 Glass transition temperature *versus* ionic radius (of the Li^+ ion, in Li_3ClO, of the doping ion (M) in $Li_{3-2\times0.005}M_{0.005}ClO$, M = Mg^{2+}, Ca^{2+}, Sr^{2+}, Ba^{2+} and of $Li_{3-2\times0.005}M_{0.005}Cl_{0.5}I_{0.5}O$). Excluding Sr^{2+}, all glass transition temperatures were obtained by Electrochemical Impedance Spectroscopy (EIS). Ionic radii were obtained from the literature.[26]

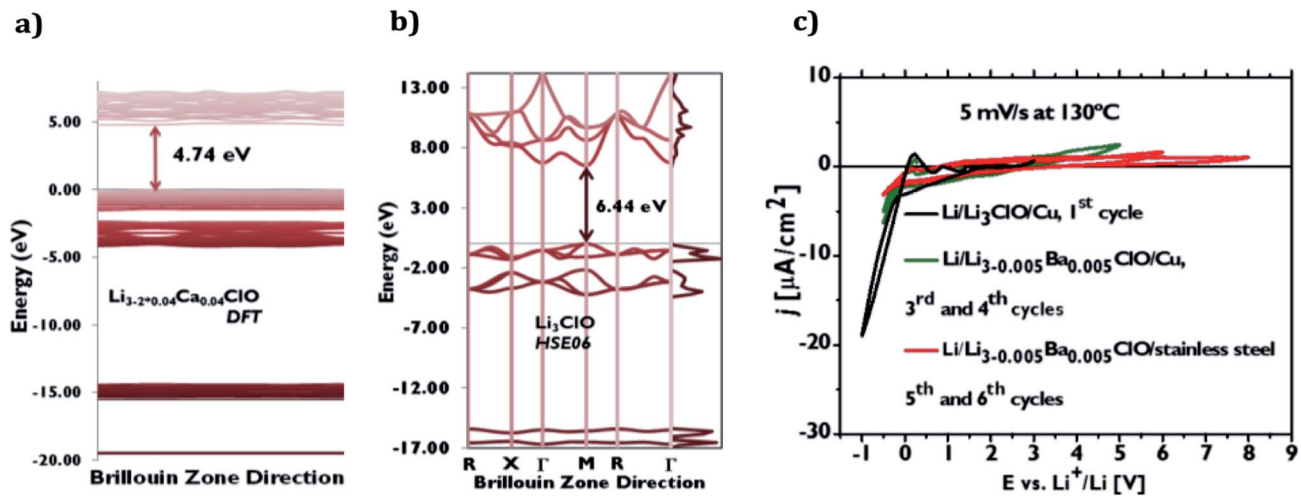

Fig. 10 Electrical properties of plain and doped Li_3ClO. (a) Calculated electronic band structure for the $Li_{3-2\times0.04}Ca_{0.04}ClO$ solid antiperovskite within the Brillouin zone directions, using DFT-GGA as implemented in VASP.[16,17] The band gap of 4.74 eV is highlighted after the Fermi level which corresponds to 0 eV. (b) Li_3ClO calculated electronic band structure within the Brillouin zone directions, using HSE06.[19] The band gap of 6.44 eV highlights the difference between E_g calculated with DFT-GGA and HSE06. (c) Voltammetry for different cells and doped electrolytes, at 130 °C, emphasizing the stability of the electrolytes up to 8 V.

very high ionic conductivities can be obtained at relatively low temperatures, *e.g.* 25 °C or lower, in high ionic radius doped glassy samples.

Fig. 12 shows the ionic conductivities for solid-like and supercooled liquid samples of plain and doped antiperovskites. In Fig. 12a, not only can the glass transitions be observed, but also the ionic conductivity hysteresis resulting from heating the followed by cooling can be observed.

A peak immediately before the ergodicity breaking transition is observed as well. Ionic conductivity dispersion, probably due to decoupling of diffusivity from viscosity,[11] is observed in the non-Arrhenius regime in Fig. 12a and b. For a material with ionic conductivity,σ, that can be measured above and below T_g, the extrapolated data for the σT term in the two domains should give identical values when the temperature, T, approaches infinity. This finding is verified in the current work and can be observed in Fig. 13.

Li_3ClO behaves as a solid-like glass (following Arrhenius law) below T_g; above T_g it becomes a supercooled liquid showing a non-Arrhenius behavior. A similar kind of behavior was observed for the doped material, although this behavior depends on the history of the material as well as it may be observed from the comparisons between the 2nd and 4th cycles in Fig. 12b for $Li_{3-2\times0.005}Ba_{0.005}ClO$. Moreover, doping is not necessary to obtain a glass, but it is helpful to get it at lower temperatures.

A $Li_{3-2\times0.005}Ba_{0.005}ClO$ sample that slowly cooled down after the 3rd heating/cooling cycle – submitted to EIS measurements

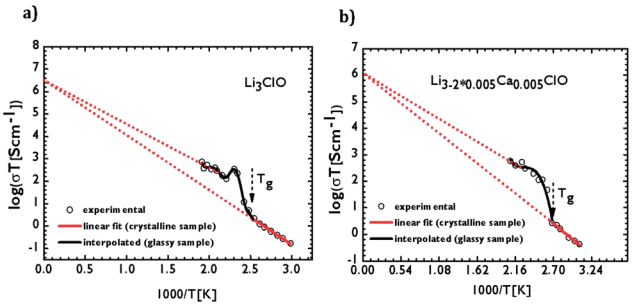

Fig. 13 log(σT) *versus* 1000 T^{-1} graphs, to highlight identical values for the extrapolated data of the σT term in the solid-like glass and supercooled liquid domains when the temperature, T, approaches infinity. (a) For a sample of Li_3ClO. (b) For a sample of $Li_{3-2\times0.005}Ca_{0.005}ClO$.

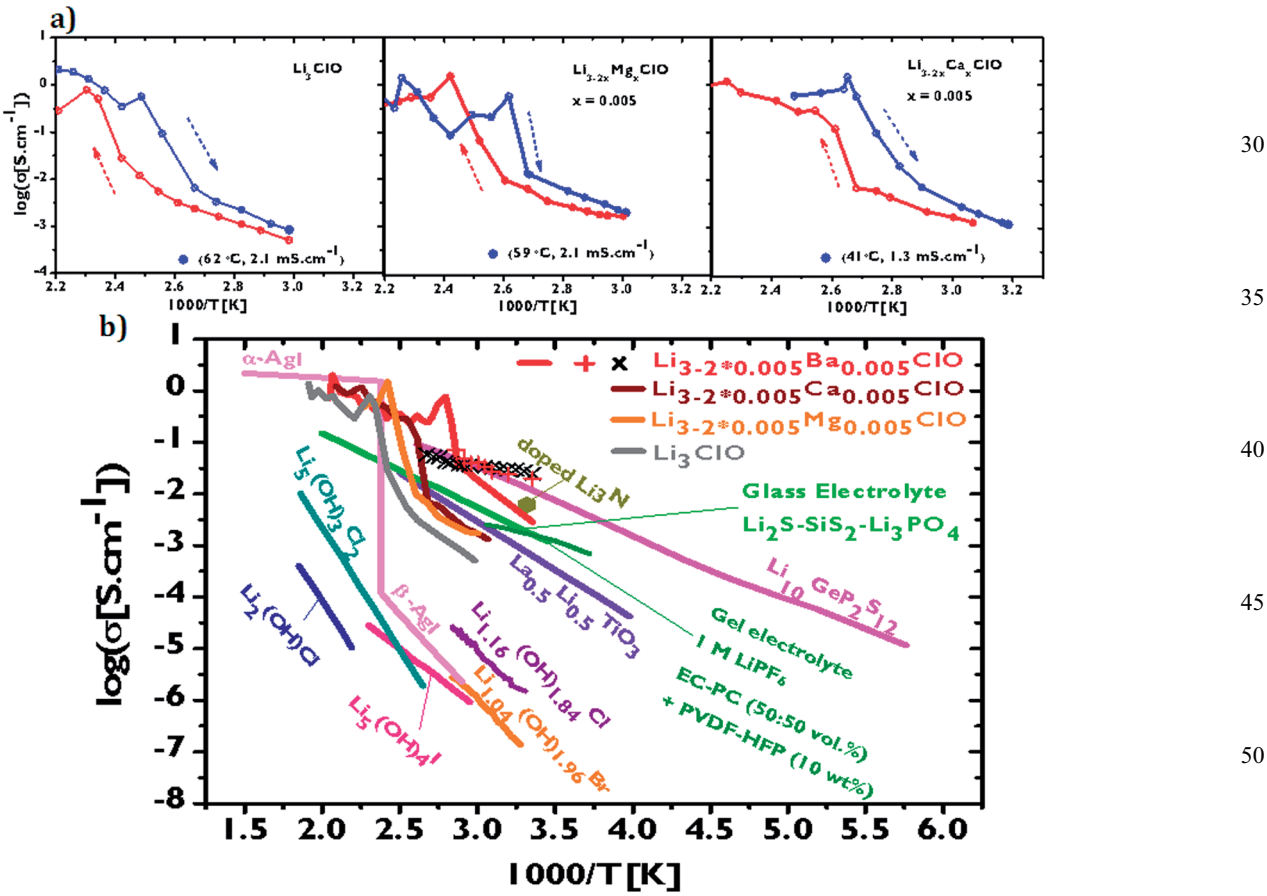

Fig. 12 Ionic conductivities of plain and doped Li_3ClO. (a) Logarithm of the ionic conductivity of Li_3ClO, $Li_{3-2\times0.005}Mg_{0.005}ClO$ and $Li_{3-2\times0.005}Ca_{0.005}ClO$ *versus* 1000/T^{-1} [K] during heating and cooling. (b) Comparison between the logarithm of the ionic conductivities of hydroxides[12–14] that can be formed during $Li_{3-2\times x}M_xHalO$ synthesis; some known solid electrolytes[5,27–30] and a gel electrolyte commonly used in Li-ion batteries;[31] Li_3ClO and $Li_{3-2\times0.005}M_{0.005}ClO$ (M = Mg, Ca and Ba) during heating. Line and symbols +, × for $Li_{3-2\times0.005}Ba_{0.005}ClO$ glassy samples in their 2nd, 3rd and 4th heating/cooling cycles, respectively. EIS measurements were performed during heating.

on heating – shows unusually high ionic conductivity at 25 °C as expected and as it is shown in Fig. 12b (+ symbols). In Fig. 14 the pseudo-Arrhenius curve for the latter sample in the 4th cycle can be observed. Although linear behavior is not expected, at least above T_g, activation energies as low as 0.06 eV can be observed in the temperature range of 35 °C to 74 °C. The glass transition can be observed in Fig. 12b (× symbols) and in Fig. 14, although it is much smoother than in previous cycles, probably indicating higher similitude between the supercooled liquid and the solid-like material highlighting that the glass dynamics depends very highly on the cooling rate, among other factors (Fig. 15).

Other systems being investigated by others as battery electrolytes include oxide perovskite such as $La_{0.5}Li_{0.5}TiO_3$;[27] hydroxides containing Li and halides,[12–14] lithium nitride,[28] glassy material such as Li_2S–SiS_2–Li_3PO_4 (ref. 29) and AgI in its allotropes (low temperature β-AgI and high temperature α-AgI).[30] Nonetheless, for lithium batteries, the glassy phase, $Li_{3-2\times x}M_xHalO$, offers higher ionic conductivity as it is shown in Fig. 12b and superior chemical stability compared with those materials, as shown in Fig. 10. Furthermore, unlike Ti and Ge containing materials, $Li_{3-2\times x}M_xHalO$ does not react with lithium-metal and offers a wider window of electrochemical stability.

Moreover, from the air, the only element that should be avoided – at least after synthesizing a highly conductive glass – should be water vapor, which makes our electrolyte an excellent candidate to be used in lithium-air batteries with lithium-metal anode.

Doping with Ba^{2+} enhances this effect even further since a larger doping ion radius in this case results in higher anisotropy of the lattice, and this seems to be in favor of higher ionic conductivity. However, such an enhancement is limited by other mechanisms such as the hopping ion trapping in the vicinity of the doping ion; which is less likely to occur in $Li_{3-2\times0.005}Ba_{0.005}Cl_{0.5}I_{0.5}O$ since the presence of I^- in the center of the cube will expand the lattice, as described to occur in $Li_3Cl_{0.5}Br_{0.5}O$[23] (Fig. 16).

A symmetric Li/$Li_{3-2\times0.005}Ca_{0.005}ClO$/Li cell was configured to demonstrate the cyclability and long-term compatibility of $Li_{3-2\times0.005}Ca_{0.005}ClO$ with metallic lithium. Fig. 17a and b shows the voltage profile of the cell cycled near room temperature, at 44 °C. At this temperature, the cell presented a voltage of 46.0 mV at a current density of 0.1 mA cm^{-2}. The direct current (dc) conductivity derived from the symmetric cell was 0.27 mS cm^{-1} – obtained by chronopotentiometry as shown in Fig. 17a and b – which is relatively close to the alternating-current (ac) conductivity of 0.85 mS cm^{-1} obtained from electrochemical impedance spectroscopy measurements extrapolated for 44 °C. Small interfacial resistance between the lithium electrode and the solid electrolyte was observed, further confirming that the $Li_{3-2\times0.005}Ca_{0.005}ClO$ is completely compatible with metallic lithium. The cell showed excellent cyclability at 44 °C as illustrated in Fig. 17a and b, not showing signs of resistance increase during more than 460 h being much more stable than many other electrolytes.[32] These results prove

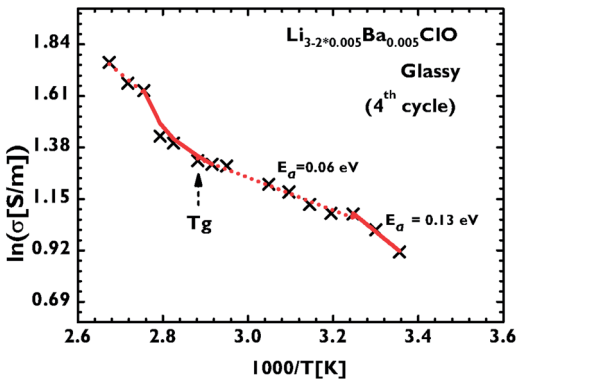

Fig. 14 Pseudo-Arrhenius plot and "apparent" activation energies for a $Li_{3-2\times0.005}Ba_{0.005}ClO$ sample during the 4th heating/cooling cycle. The sample was submitted to an EIS cycle on every heating step. The sample was glassy and therefore an Arrhenius behavior at least above T_g is not expected.

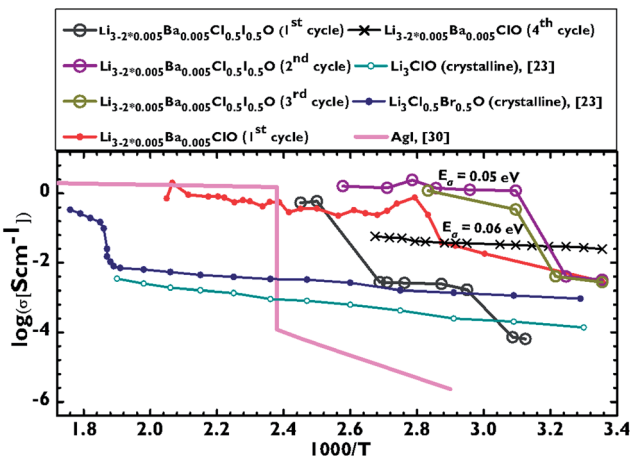

Fig. 15 Ionic conductivities of plain and doped Li_3ClO. Logarithm of the ionic conductivity of Li_3ClO,[23] $Li_3Cl_{0.5}Br_{0.5}O$,[23] AgI,[30] $Li_{3-2\times0.005}Ba_{0.005}ClO$ (1st and 4th cycles) and $Li_{3-2\times0.005}Ba_{0.005}Cl_{0.5}I_{0.5}O$ (1st to 3rd cycles) *versus* 1000 T^{-1} [K] during heating.

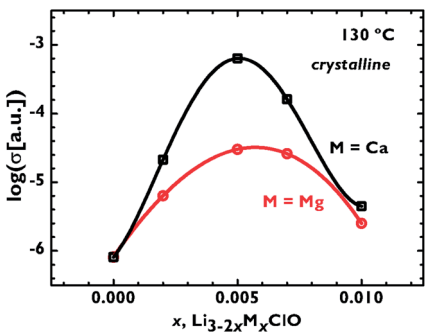

Fig. 16 The experimental ionic conductivity *versus* concentration for $Li_{3-2\times x}Ca_xClO$ and $Li_{3-2\times x}Mg_xClO$. These results were obtained in the stainless steel non-optimized cell described in the Experimental section. Electrodes were of stainless steel. The sample cannot be pressure tight as in the gold cell, and most likely the samples did not become glasses.

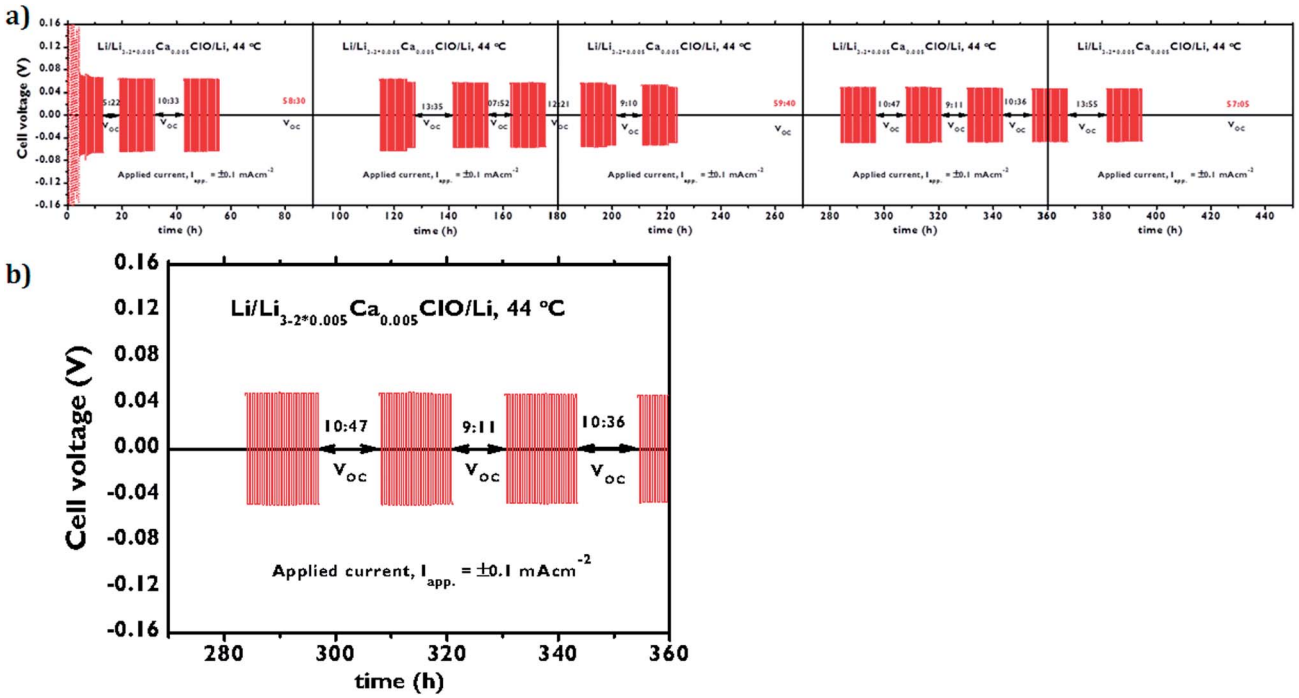

Fig. 17 Cycle stability of the solid electrolyte *versus* the Li-metal. (a) Chronopotentiometry emphasizing cycling stability of a Li/$Li_{3-2\times0.005}Ca_{0.005}ClO$/Li cell. V_{oc} stands for open circuit voltage. (b) Zoom of the graph in (a) showing the stability of the Li/$Li_{3-2\times0.005}Ca_{0.005}ClO$/Li cell.

the ability of the glass to be used in Li batteries for electronic devices.

Moreover, the ionic conductivity increases until above 220 h, as shown in Fig. 17a, indicating that, even at 44 °C, the sample will become partially amorphous eventually due to electrochemical cycling.

The solid electrolyte Li_3ClO structure employs abundant Li^+ (high concentration of mobile charge carriers) and non-toxic elements and is easily processed, using wet chemistry at relatively low temperatures (240 °C to 310 °C), which is another argument for inexpensive and environmentally friendly fabrication. Samples were annealed in a pressure tight wafer of Au – in the cell setup – at up to 250 °C. Seldom was it needed more than one cycle for the sample to become partially vitreous and highly conductive. A glassy surface and structure is visible to the eyesight after heating and cooling in Fig. 7 and as denoted in Fig. 2. The sample can become transparent on melting.

It is likely that the precursor hydroxides have an important role in product formation promoting the contact between the reagent compounds powders. These hydroxides are anti-perovskite structures, most of them following the general formula $Li_{3-n}(OH_n)Hal$.[12–14] Their ionic conductivities are considerably smaller than the $Li_{3-2\times x}M_xHalO$ vitreous electrolytes. In fact, the hydroxide recurrently formed was $Li_5(OH)_3Cl_2$[14] and/or $Li_4(OH)_3Cl$[30] but it transforms into $Li_{3-2\times x}M_xHalO$ after the first cycle as it can be inferred from Differential Scanning Calorimeter (DSC) measurements shown in Fig. 3.

The glass transition of $Li_{3-2\times0.005}Mg_{0.005}ClO$ in DSC measurements seems to occur at T_g ~136 °C as observed in Fig. 3, which is in agreement with the ionic conductivity results. Melting of $Li_{3-2\times0.005}Mg_{0.005}ClO$ occurs at T_m = 269 °C as the correspondent endothermic peak demonstrates in Fig. 3. A glass transition, T_g, is linked *via* an empirical relationship with the melting temperature T_m, $T_g \sim (2/3)T_m$.[33] We obtained, $T_g\,T_m^{-1}$ ~0.75, by means of DSC, and $T_g\,T_m^{-1}$ ~0.71, by conductivity measurements, which is a good approximation to the empirical factor of 0.67.

The phonon density of states was calculated using DFT and compared with Incoherent Inelastic Neutron Spectroscopy (IINS) spectra. The role of the lattice during hopping and diffusion was established experimentally as a function of electrodes' temperature, voltage and applied frequency. Most of the vibration modes maintain a constant intensity with the applied frequency as observed in Fig. 18.

The effect is likely to be associated with the crystalline behavior since the experimental conditions were not favorable to glass formation.

For 320–380 cm^{-1} wavenumbers (~1013 Hz), the intensity varies with the applied frequency, being higher at f = 100 Hz and lower at $f = 10^4$ Hz.

This is most likely the jump frequency (~1013 Hz) as the eigenvectors associated with phonons suggest, which implies that at higher frequencies more ions have jumped already.

It is important to mention that the Li_3ClO-crystalline density is as low as 2.07 g cm^{-3} ($Li_{3-2\times0.005}Ca_{0.005}ClO$-crystalline is 2.09 g cm^{-3} and $Li_{3-2\times0.005}Ba_{0.005}ClO$-crystalline is 2.28 g cm^{-3}). At 200 °C Li_3ClO density is ~1.96 g cm^{-3} although we cannot assure that the sample was completely amorphous. Liquid electrolytes in lithium-ion batteries consist of lithium

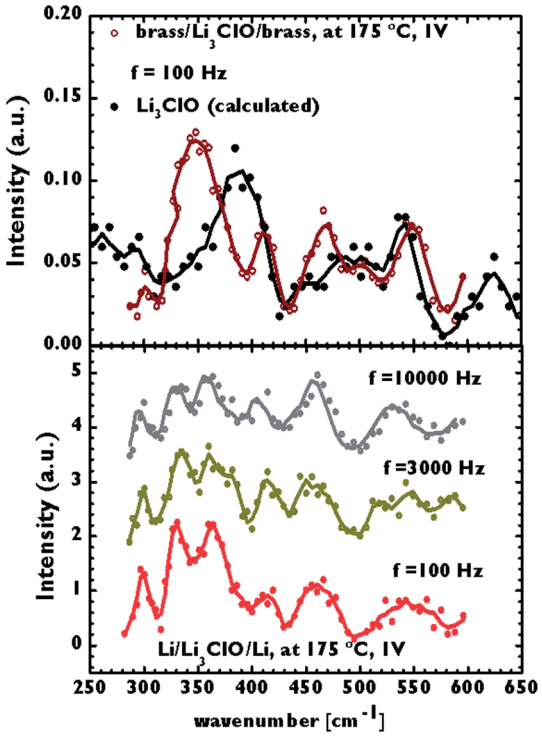

Fig. 18 Lattice vibration spectra of the Li_3ClO. Above: the calculated spectrum and IINS for a brass/Li_3ClO/brass cell (blocking electrodes). Below: the IINS for a Li/Li_3ClO/Li cell. The dependence from the applied frequency of the intensity of the spectra peaks highlights the jump frequency. This effect is notorious for the peaks around 350 cm^{-1}. In the calculated spectra, incoherent cross-sections of each element were not weighed. Additionally, calculations did not take into account the overtones.

salts, such as $LiPF_6$ (1.50 g cm^{-3}) or $LiClO_4$ (2.42 g cm^{-3}) in an organic solvent, such as ethylene carbonate (1.3 g cm^{-3}) or dimethyl carbonate (1.07 g cm^{-3}).

Although the cell will not be lighter just by replacing the liquid by an equal volume of the solid electrolyte and even if moisture has to be avoided likewise; merely a thin film of solid electrolyte is needed with no separator or sophisticated packaging resulting in a lighter battery.

Conclusions

The present results show that the new $Li_{3-2x}M_xHalO$ glassy electrolyte (in which M is a higher valent cation like Mg^{2+}, Ca^{2+} or especially Ba^{2+}, and Hal is a halide like Cl^-, or a mixture of halides like Cl^- and I^-) has an extremely high ionic conductivity that is well above the lithium-ion conductivity of any other lithium superionic conductor at $T = 25$ °C (25 mS cm^{-1}). It is the first time that a glass formed from an antiperovskite crystal is presented. It is likely to have other applications in the future or to serve as model for the synthesis of other superionic glasses obtained from antiperovskite precursors. In addition, this new electrolyte is chemically very stable with respect to Li-metal (more than 260 cycles), proving that it can be used in consumer electronic devices, and it is a light, good electronic insulator, non-flammable and contains no pollutants. Moreover, this novel electrolyte is easy to synthesize, thermally stable and electrochemically stable at least up to 8 V. It is thus promising for applications requiring batteries with high powers and energy densities, especially, for hybrid electric and pure electric vehicles.

Acknowledgements

We are grateful to FCT – Portugal and the FEDER/COMPETE for the PTDC/CTM/099461/2008 and PEst-C/EME/UI0285/2013 project support and instrumentation and to LNEG for laboratory facilities and support. This work has benefited from the use of FDS at LANSCE, LANL, USA, funded by DOE, DE-AC52-06NA25396. MHB is grateful to Y. Zhao, L. L. Daemen and to the Laboratory-Directed Research and Development (LDRD) program of Los Alamos National Laboratory for initial support conducing to neutron scattering experiments.

Notes and references

1 M. Tatsumisago and A. Hayashi, *Solid State Ionics*, 2012, **225**, 342.
2 N.-S. Choi, Z. Chen, S. A. Freunberger, X. Ji, Y.-K. Sun, K. Amine, G. Yushin, L. F. Nazar, J. Cho and P. G. Bruce, *Angew. Chem., Int. Ed.*, 2012, **51**, 9994.
3 Z. Chen, Y. Qini, Y. Ren, W. Lu, C. Orendorff, E. P. Roth and K. Amine, *Energy Environ. Sci.*, 2011, **4**, 4023.
4 Ohara Inc. 2013 [last visit, Oct. 2013]. http://www.ohara-inc.co.jp/en/product/electronics/licgc.html.
5 N. Kamaya, K. Homma, Y. Yamakawa, M. Hirayama, R. Kanno, M. Yonemura, T. Kamiyama, Y. Kato, S. Hama, K. Kawamoto and A. A. Mitsui, *Nat. Mater.*, 2011, **10**, 682.
6 Y. Mo, S. P. Ong and G. Ceder, *Chem. Mater.*, 2012, **24**, 15.
7 S. Kondo, K. Takada and Y. Yamamura, *Solid State Ionics*, 1992, **53–56**(2), 1183.
8 A. Hayashi, H. Yamashita, M. Tatsumisago and T. Minami, *Solid State Ionics*, 2002, **148**, 381.
9 ISO 11357–2: Plastics – Differential Scanning Calorimetry (DSC) – Part 2: Determination of glass transition temperature, 1999.
10 J.-P. Hansen and I. R. McDonald, *Theory of Simple Liquids*, Elsevier, 2007.
11 C. A. Angell, K. L. Ngai, G. B. McKenna, P. F. McMillan and S. W. Martin, *J. Appl. Phys.*, 2000, **88**(6), 3113–3157.
12 G. Schwering, A. Hönnerscheid, L. van Wüllen and M. Jansen, *ChemPhysChem*, 2003, **4**, 343.
13 P. Hartwig, A. Rabenau and W. Weppner, *J. Less-Comm. Met.*, 1981, **78**, 227.
14 P. Hartwig and W. Weppner, *Solid State Ionics*, 1981, **3-4**, 249.
15 A. Hönnerscheid, J. Nuss, C. Mühle and M. Jansen, *Z. Anorg. Allg. Chem.*, 2003, **629**, 317.
16 P. E. Blochl, *Phys. Rev. B: Condens. Matter Mater. Phys.*, 1994, **50**, 17953.
17 G. Kresse and J. Furthmüller, *Phys. Rev. B: Condens. Matter Mater. Phys.*, 1996, **54**(16), 11169.

18 J. P. Perdew and Y. Wang, *Phys. Rev. B: Condens. Matter Mater. Phys.*, 1992, **45**, 13244.
19 J. Heyd, G. E. Scuseria and M. Ernzerhof, *J. Chem. Phys.*, 2003, **118**(18), 8207.
20 K. Parlinski, Z. Q. Li and Y. Kawazoe, *Rev. Lett.*, 1997, **78**, 4063.
21 E. Wimmer, W. Wolf, J. Sticht, P. Saxe, R. Najafabadi and G. A. Young, *Phys. Rev. B: Condens. Matter Mater. Phys.*, 2008, **77**, 134305.
22 C. A. Angell, *Chem. Rev.*, 1990, **90**, 523.
23 Y. Zhao and L. L. Daemen, *J. Am. Chem. Soc.*, 2012, **134**, 15042.
24 Y. Zhang, Y. Zhao and C. Chen, *Phys. Rev. B: Condens. Matter Mater. Phys.*, 2013, **87**, 134303.
25 M. H. Hebb, *J. Chem. Phys.*, 1952, **20**, 185.
26 R. D. Shannon, *Acta Crystallogr.*, 1976, **32**, 751.
27 Y. Inaguma, C. Liquan, M. Itoh and T. Nakamura, *Solid State Commun.*, 1993, **86**, 689.
28 T. Lapp, S. Skaarup and A. Hooper, *Solid State Ionics*, 1983, **11**, 97.
29 K. Takada, N. Aotani and S. Kondo, *J. Power Sources*, 1993, **43**, 135.
30 H. Mehrer, *Diffusion in Solids Fundamentals, Methods, Materials, Diffusion-Controlled Processes*, Springer Series in Solid-State Sciences, 1st edn, vol. 155, 2007.
31 J. Y. Song, Y. Y. Wang and C. C. Wan, *J. Electrochem. Soc.*, 2000, **147**, 3219.
32 Z. Liu, W. Fu, E. A. Payzant, X. Yu, Z. Wu, N. J. Dudney, J. Kiggans, K. Hong, A. J. Rondinone and C. Liang, *J. Am. Chem. Soc.*, 2013, **135**, 975.
33 S. Sakka and J. D. Mackenzie, *J. Non-Cryst. Solids*, 1971, **25**, 145.